ROYAL SOCIETY OPEN SCIENCE

royalsocietypublishing.org/journal/rsos

Research

**Cite this article:** Ji A, Kasting JF, Cooke GJ, Marsh DR, Tsigaridis K. 2023 Comparison between ozone column depths and methane lifetimes computed by one- and three-dimensional models at different atmospheric $O_2$ levels. *R. Soc. Open Sci.* **10**: 230056. https://doi.org/10.1098/rsos.230056

Received: 30 January 2023
Accepted: 13 April 2023

**Subject Category:**
Earth and Environmental Science

**Subject Areas:**
atmospheric chemistry/atmospheric science

**Keywords:**
atmospheric chemistry, ozone layer, methane lifetime, proterozoic atmosphere, one-dimensional model, three-dimensional model

**Author for correspondence:**
A. Ji
e-mail: azj64@psu.edu

Electronic supplementary material is available online at https://doi.org/10.6084/m9.figshare.c.6617700.

THE ROYAL SOCIETY PUBLISHING



# Comparison between ozone column depths and methane lifetimes computed by one- and three-dimensional models at different atmospheric $O_2$ levels

A. Ji[1], J. F. Kasting[1], G. J. Cooke[2], D. R. Marsh[2,3] and K. Tsigaridis[4,5]

[1]Department of Geosciences, Penn State University, University Park, PA 16802, USA
[2]School of Physics and Astronomy, University of Leeds, Leeds LS2 9JT, UK
[3]National Center for Atmospheric Research, Boulder, CO 80301, USA
[4]Center for Climate Systems Research, Columbia University, New York, NY 10025, USA
[5]NASA Goddard Institute for Space Studies, 2880 Broadway, New York, NY 10025, USA

AJ, 0000-0002-9152-1287; GJC, 0000-0001-6067-0979; DRM, 0000-0001-6699-494X; KT, 0000-0001-5328-819X

Recently, Cooke *et al*. (Cooke *et al*. 2022 *R. Soc. Open Sci.* **9**, 211165. (doi:10.1098/rsos.211165)) used a three-dimensional coupled chemistry-climate model (WACCM6) to calculate ozone column depths at varied atmospheric $O_2$ levels. They argued that previous one-dimensional (1-D) photochemical model studies, e.g. Segura *et al*. (Segura *et al*. 2003 *Astrobiology* **3**, 689–708. (doi:10.1089/153110703322736024)), may have overestimated the ozone column depth at low $pO_2$, and hence also overestimated the lifetime of methane. We have compared new simulations from an updated version of the Segura *et al*. model with those from WACCM6, together with some results from a second three-dimensional model. The discrepancy in ozone column depths is probably due to multiple interacting parameters, including $H_2O$ in the upper troposphere, lower boundary conditions, vertical and meridional transport rates, and different chemical mechanisms, especially the treatment of $O_2$ photolysis in the Schumann–Runge (SR) bands (175–205 nm). The discrepancy in tropospheric OH concentrations and methane lifetime between WACCM6 and the 1-D model at low $pO_2$ is reduced when absorption from $CO_2$ and $H_2O$ in this wavelength region is included in WACCM6. Including scattering in the SR bands may further reduce this difference. Resolving these issues can be

accomplished by developing an accurate parametrization for $O_2$ photolysis in the SR bands and then repeating these calculations in the various models.

# 1. Introduction

The calculation of ozone column depth as a function of atmospheric $O_2$ concentration has been performed multiple times over the past 40 years using one-dimensional (1-D) photochemical models. Several of these calculations [1–3] have been done by the Kasting group. We refer to the current version of that model as the 'standard' 1-D model (see §2). Recently, Cooke *et al*. [4], henceforth C22, performed a similar calculation using a three-dimensional (3-D) coupled chemistry-climate model (WACCM6). They found substantially lower ozone column depths at lower $pO_2$ levels. For example, at 0.01 times the present atmospheric level (PAL) of $O_2$, Segura *et al*. [3] calculated 124 Dobson units (DU), whereas C22 [4] calculated a mean column depth of just 66 DU—almost a factor of two lower. This comparison is shown in figure 1. C22 [4] argued, correctly, that 3-D models should be able to do a better job on this problem than 1-D models because ozone column depths are affected by atmospheric transport, e.g. the Brewer–Dobson circulation in the stratosphere that blows ozone from the tropics towards the poles, as well as vertical transport that carries ozone downward from the stratosphere to the troposphere. Meridional transport is absent in 1-D models, and vertical transport is fixed, so model geometry almost certainly contributes to the observed discrepancies in ozone column depth. The 3-D model also has a variable tropopause height (higher at the equator, lower towards the poles), which is difficult to simulate in one dimension.

To complicate matters, an independent 3-D investigation of this problem by Way *et al*. [6] using the ROCKE-3D model produced results similar to the previous 1-D calculations (see C22 [4] fig. 6 and our figure 1), for example, 123 DU at 0.01 PAL $O_2$. Another study published in late 2022 by Jaziri *et al*. [5] shows both 1-D and 3-D calculations on the ozone column depths at low $pO_2$ (less than or equal to 0.005 PAL) which are much closer to WACCM6 (see black curves in figure 1). A preliminary intercomparison study between the 1-D, WACCM6 3D and ROCKE-3D models suggests that multiple factors contribute to the differences in the modelled ozone column depths. The parametrization of $O_2$ photolysis within the Schumann–Runge (SR) bands (175–205 nm) plays a significant role in causing this $O_3$ discrepancy, but more detailed work needs to be done to quantify its effect and the effects of other possible factors.

C22 [4] also argued that because of the lower ozone column depths at low $pO_2$, the lifetime of $CH_4$ should be shorter than previously estimated. That is because less ozone means that more solar near-UV radiation would reach the troposphere, creating more OH to destroy $CH_4$ through the following two processes: (i) radiation below approximately 230 nm can directly dissociate gaseous $H_2O$, creating OH radicals that then react with $CH_4$; (ii) wavelengths between 200 and 310 nm can photolyse tropospheric ozone, creating $O(^1D)$ radicals that generate more OH by reacting with $H_2O$: $O(^1D) + H_2O \rightarrow 2$ OH. As a result, C22 [4] concluded that previous suggestions that methane may have played a significant role in warming the Proterozoic climate are probably incorrect. We demonstrate here that differences in the parametrization of $O_2$ photolysis together with whether to consider the absorption by $H_2O$ and $CO_2$ at SR wavelengths account for much of the difference in the methane lifetime, so ruling out methane as an important Proterozoic greenhouse gas would be premature at this time.

# 2. Brief model descriptions

## 2.1. One-dimensional photochemical model

The current (Kasting group) 1-D photochemical model is taken directly from Liu *et al*. [7]. It extends from the ground up to 100 km altitude in 1 km increments. This model uses a fully implicit, reverse Euler method to solve the coupled continuity and flux equations, along with a two-stream multiple scattering algorithm from Toon *et al*. [8] to calculate the radiative transfer of incident sunlight for the calculation of photolysis rates only. Three temperature profiles are specified for 1 PAL, 0.1 PAL and $pO_2$ of 0.01 PAL and below (figure 2*a*). The modern temperature profile is obtained from US Standard Atmosphere, 1976. These profiles are similar to those calculated by Segura *et al*. [3] using a radiative-

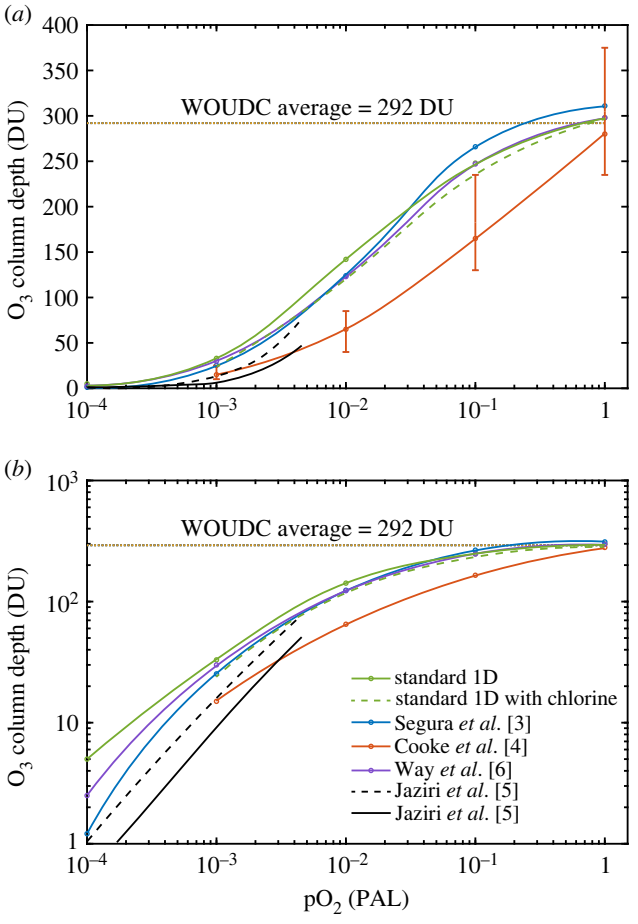


**Figure 1.** $O_3$ column depths at varied $pO_2$ levels based on calculations by different groups. Our standard 1-D model is shown by the solid green curve in (*a*) a linear scale and (*b*) a log scale. The standard 1-D model with chlorine is shown by the dashed green curve. 'WOUDC' stands for 'World Ozone and UV Radiation Data Center'. Note that we only did calculations at 1 PAL, 0.1 PAL, 0.01 PAL and 0.001 PAL, so the curves do not imply continuous results. In (*a*), the orange curve shows the mean value from WACCM6, with maximum and minimum values (at different longitudes) indicated by the vertical bars. Jaziri *et al*. [5] calculated the ozone column depths for very low $pO_2$ (less than or equal to 0.005 PAL) which are also shown here in black curves (dashed black curve for their 1-D calculations at 40° solar zenith angle and solid black curve for their 3-D calculations).

convective model. For $pO_2 < 0.1$ PAL, we kept the same tropospheric temperature profile and assumed that the stratosphere was isothermal. The model includes standard atmospheric chemistry for C, H, O, N, S species, and we refer to it here as the 'standard' 1-D model. The main code includes 30 long-lived species, 28 short-lived species and 222 chemical reactions. Some calculations were also performed with chlorine chemistry included, based on the reaction scheme in Stanton *et al*. [9]. Heterogeneous chemistry is not included in the chemical scheme. The treatment of lower boundary conditions for biogenic trace gases ($CH_4$, $N_2O$, CO, $CH_3Cl$ and $H_2$) is the same as in Liu *et al*. [7] and Segura *et al*. [3]. These trace gases are fixed at observed values for the modern atmosphere simulations. The model returns the surface flux needed to sustain the present values, and we hold these surface fluxes constant and allow the mixing ratios of the various trace gases to float at lower $pO_2$ (see electronic supplementary material for details). This low $pO_2$ cannot be lower than $10^{-4}$ PAL in the 1-D model as we design for a well-mixed $O_2$ atmosphere. Two important updates have been made, though: (i) eight-point Gaussian integration over the sunlit hemisphere is used in the current 1-D model to more accurately calculate globally averaged photolysis rates (see electronic supplementary material); (ii) new $H_2O$ cross sections extrapolated to 233 nm by Ranjan *et al*. [10] are included in the current model. Most of the model intercomparisons in this paper are between the updated 1-D model (the standard run) and the WACCM6 3-D model.

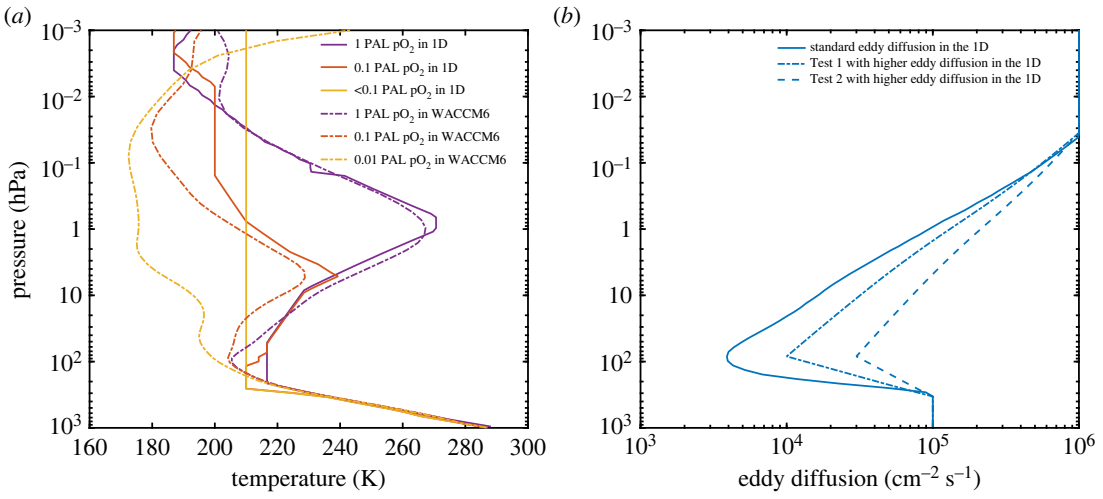


**Figure 2.** (*a*) Temperature profiles used in the 1-D model and WACCM6 3-D model; different colours represent different $pO_2$; solid curves represent 1-D temperature profiles and dashed-dotted curves represent WACCM6 temperature profiles. (*b*) Eddy diffusion profile used in the 1-D model and higher eddy diffusion tests.

## 2.2. WACCM6 model description

The Whole Atmosphere Community Climate Model version 6 (WACCM6) is a configuration of the Community Earth System Model version 2 (CESM2). WACCM6 is a 3-D model which couples together land, land-ice, ocean, sea-ice and atmosphere sub-models [11]. In C22 [4], the simulations used modified configurations of the standard pre-industrial control (the so-called BWma1850 'compset'). The atmospheric model uses the finite volume dynamical core [12] with horizontal resolution of 1.875° in latitude by 2.5° in longitude. There were 70 levels in the vertical using a hybrid-sigma coordinate system from the surface to a pressure of $6 \times 10^{-6}$ hPa (approx. 140 km) [11]. At this resolution, the quasi-biennial oscillation (QBO) is produced via a specified dynamical forcing.

The coupled chemistry used in WACCM6 is based on the Model for Ozone and Related chemical Tracers (MOZART; [13–16]). This particular WACCM6 set-up includes 98 chemical species, 208 chemical reactions and 90 photolysis reactions. Twenty-two long-lived species are calculated explicitly; the other 75 species are calculated using a fully implicit Euler backward method with Newton–Raphson iteration [16]. $N_2$ is considered to be invariant. For $O_3$, Chapman chemistry is included, as well as the $HO_x$, $NO_x$, $BrO_x$ and $ClO_x$ species which are involved in catalytic cycles that destroy $O_3$. Each constituent is solved individually rather than using a family approach, as in the ROCKE-3D model described below. The atmospheric time step is 30 min. Apart from $O_2$, lower boundary conditions were kept the same as in the 1-PAL $O_2$ run, whether that was through a fixed flux or a fixed mixing ratio. This means that fixed volume mixing ratios were generally assumed for $CH_4$ ($8.08 \times 10^{-7}$), $N_2O$ ($2.73 \times 10^{-7}$), $CH_3Cl$ ($4.57 \times 10^{-10}$) and $CH_3Br$ ($5.30 \times 10^{-12}$). Two alternative calculations used fixed fluxes for $CH_4$. The standard upper boundary conditions were scaled in order to enable consistent calculations in the upper atmosphere. See C22 [4] for more details. Three new simulations (not described in C22 [4]) were done with a lower amount of methyl chloride, $CH_3Cl$ (see §5.2), and new simulations at 0.1, 0.01 and 0.001 PAL included the lower boundary conditions from the Kasting 1-D model with SR-band absorption for $CO_2$ and $H_2O$ with updated cross sections.

Reaction rates for WACCM6 were updated to include the Burkholder *et al*. [17] recommendations [11]. Photolysis rates are calculated via a lookup table from the tropospheric ultraviolet and visible (TUV) radiation model [15]. The $O_2$ photolysis rate ($JO_2$) below 200 nm is calculated for Lyman-α, Schumann–Runge continuum (SRC), and Schumann–Runge bands (SRB), using parametrizations from Chabrillat & Kockarts [18], Brasseur & Solomon [19] and Koppers & Murtagh [20], respectively. JNO is parametrized in the SRB using Minschwaner & Siskind [21]. Scattering is included longward of 200 nm, but not included for $O_2$ in the SRB. Additionally, scattering takes place for solar zenith angles beyond 90°. The Koppers & Murtagh [20] scheme is known to be more accurate than the Allen & Frederick [22] band model on which the Kasting group parametrization is based (but see more below on how that parametrization is actually implemented).

WACCM6 simulations have been shown to reproduce the quasi-biennial oscillation (at a higher atmospheric resolution than simulated here), stratospheric sudden warmings, the evolution of Southern Hemisphere springtime ozone depletion over the twentieth century, the water vapour tape recorder in the tropics, the Brewer–Dobson circulation and the observed ozone distribution with latitude [11]. Furthermore, the model has been used to reproduce the evolution of the ozone layer, including the formation of the ozone hole and its recovery [23,24], with observations within the variability limits predicted from the simulations, and larger biases occurring in free-running simulations when compared with specified dynamics simulations [11]. Additionally, WACCM6 is able to reproduce the observed historical evolution of global mean surface temperature anomalies.

### 2.3. ROCKE-3D model description

The Resolving Orbital and Climate Keys of Earth and Extraterrestrial Environments with Dynamics (ROCKE-3D) version 1.0 general circulation model (GCM) was described in Way *et al*. [6], and only a brief description will be provided here. ROCKE-3D is the generalized version of GISS ModelE version 2.0 [25], used in the Coupled Model Intercomparison Project phase 5 (CMIP5), for application to non-modern Earth terrestrial planets. It has been extended to use the Suite Of Community Radiative Transfer codes based on Edwards & Slingo (SOCRATES; [26,27]), among other updates [6]. For the simulations used here, the default model radiative transfer code was used for performance, since the atmosphere was largely similar to that of modern Earth.

The resolution of the model was 2° in latitude by 2.5° in longitude, with a vertical sigma layer coordinate system from the surface to the stratopause, at about 65 km altitude. The time step of the model is 30 min. In the low-$O_2$ simulations performed, the atmospheric composition represented that of the pre-industrial atmosphere in all respects except that of lower $O_2$ amounts. $O_2$ changes were not allowed to affect radiative transfer in climate calculations, i.e. all simulations used present-day $O_2$ levels, contrary to $O_3$ changes that were taken into account in the radiation calculations. On the other hand, for the photolysis rate calculations, both $O_2$ and $O_3$ changes were included.

The chemical scheme used is a modified version of the Carbon Bond Mechanism version 4 (CBM4; [28]) as described by Shindell *et al*. [29,30]. The chemical scheme includes an explicit parametrization of $O_x$, $NO_x$, $HO_x$ and $CH_4$ reactions, and a heavily parametrized scheme for organic compounds with two or more carbon atoms. In addition, the stratospheric chemistry of chlorine is also included [31], as it is necessary for the simulation of the ozone hole in the late twentieth century. No tropospheric chemistry of halogens is included in the model. Aerosols (primary and secondary organic carbon, black carbon, sulfate, ammonium, nitrate) are included using a bulk scheme (only aerosol mass is simulated), while sea salt and dust are described using a sectional model (Schmidt *et al*. [25] and references therein). There are two wavebands that overlap with the SR bands in the photolysis scheme, centred at 187 and 192 nm. The photolysis scheme includes Rayleigh scattering but does not include direct photolysis of $CO_2$ and $H_2O$ or absorption by these gases (CE Harman, Jr 2023, personal communication).

In simulations with prescribed atmospheric composition, long-lived greenhouse gases ($CH_4$, $N_2O$, $CO_2$, CFCs) are prescribed at the surface using an annually varying (for transient simulations only) global surface mean value, and using a prescribed latitudinal and vertical profile. When chemistry is included in the simulations, which results in atmospheric composition being calculated prognostically, this approach is only used for $CO_2$; for the other greenhouse gases (GHGs) that participate in chemistry, only the surface amounts are prescribed, while the values in the vertical are free to evolve as chemistry and dynamics dictate. An important detail is what happens at the surface: at every time step, chemistry and dynamics are allowed to modify surface values, but then these are reset to the prescribed ones. The difference between the calculated and prescribed values is saved and it can be used as a source estimate of those gases. No different treatment was introduced in this approach when the $O_2$ levels were changing across simulations.

## 3. Comparisons of ozone column depth as a function of $pO_2$

Before discussing the details about how the different models calculate the ozone column depth at varied $pO_2$, we first explain some of the parameters that may contribute to the discrepancies in the results.

We compare the temperature profiles used in the 1-D model with the globally averaged temperatures from the WACCM6 model in figure 2*a*. The atmospheric temperature at a particular pressure sets the number density of molecules and influences the rate of many chemical reactions. For the 1-D model,

**Table 1.** Ozone column depth (unit: DU) as a function of $pO_2$ from different calculations.

| no. | $pO_2$ (PAL) | 1 | 0.1 | 0.01 | 0.001 | 0.0001 |
|---|---|---|---|---|---|---|
| 1 | standard run[a] | 298 | 248 | 142 | 33 | 5 |
| 2 | standard run with chlorine species[a] | 296 | 236 | 120 | 24 | |
| 3 | Segura *et al*. [3][a] | 311 | 266 | 124 | 25.3 | 1.2 |
| 4 | Cooke *et al*. [4][b] | 279 | 169 | 66 | 18 | |
| 5 | Way *et al*. [6][b] | 298 | 247 | 123 | 30 | 2.5 |
| 6 | Jaziri *et al*. [5] 1-D | | | | 18 | 0.8 |
| 7 | Jaziri *et al*. [5][b] | | | | 8 | 0.4 |
| **sensitivity tests in the 1-D model** | | | | | | |
| 8 | a single solar zenith angle (48.2°)[a] | 268 | 224 | 127 | 24.5 | 2.8 |
| 9 | high $H_2O$ at the cold trap[a] | 287 | 236 | 128 | 24 | 3 |
| 10 | fixed $CH_3Cl$ mixing ratio (0.5 ppb)[a] | 296 | 239 | 113 | 5 | |
| 11 | fixed $CH_3Cl$ mixing ratio (0.5 ppb) without scattering and $H_2O$ and $CO_2$ absorption from 175 to 250 nm[a] | 306 | 263 | 13 | code crashed | |
| 12 | fixed $CH_3Cl$ surface flux ($2.8 \times 10^8$ $cm^{-2}s^{-1}$) without scattering and $H_2O$ and $CO_2$ absorption from 175 to 250 nm[a] | 306 | 260 | 155 | 26 | 3 |
| 13 | fixed $CH_3Cl$ surface flux ($2.8 \times 10^8$ $cm^{-2}s^{-1}$) without scattering and $H_2O$ and $CO_2$ absorption from 175 to 205 nm[a] | 298 | 273 | 172 | 29 | |
| 14 | standard 1-D run but with WACCM6 temperature profiles for 0.01 PAL and 0.001 PAL[a] | | | 153 | 40 | |
| 15 | standard 1-D run with high eddy diffusion coefficients | 339 | 273 | 142 | 32 | |
| 16 | standard 1-D run with constant NO production from the lightning | 296 | 259 | 132 | 26 | |
| **sensitivity tests in the WACCM6 3-D model** | | | | | | |
| 17 | standard WACCM6 run with 10 times lower $CH_3Cl/CH_3Br$ mixing ratio at the surface[b] | | 180 | 81 | | |
| 18 | standard WACCM6 run with a billion times lower $CH_3Cl/CH_3Br$ mixing ratio at the surface[b] | | | 85 | | |
| 19 | lower boundary conditions from 1-D model and SRB absorption for $H_2O$ and $CO_2$ included[b] | | 156 | 55 | 13 | |

[a]These calculations were done with the 1-D model described in this paper. (The standard run in the 1-D model is with eight Gauss points, new $H_2O$ cross section and low-$H_2O$ profiles.)
[b]These calculations were done with 3-D models.

we used three different temperature profiles for 1 PAL $O_2$, 0.1 PAL $O_2$ and $pO_2 < 0.1$ PAL, respectively; detailed descriptions are in §2.1. For the WACCM6 model, we show globally averaged and time-averaged temperature profiles at 1 PAL $O_2$ (purple dashed-dotted curve), 0.1 PAL $O_2$ (red dashed-dotted curve) and 0.01 PAL $O_2$ (yellow dashed-dotted curve). These global mean temperatures for the troposphere in both models are similar, whereas the stratospheric temperatures are quite different (the WACCM6 stratosphere is much colder at low $pO_2$). When we substitute the WACCM6 global mean temperature profiles for those in the 1-D model at 1% and 0.1% PAL $O_2$, we calculate even higher ozone column depths than in our standard runs (table 1), which makes sense because the rate of formation of ozone and the rates of many ozone-destroying reactions are temperature-dependent. Therefore, while

temperature differences are important for ozone column comparisons, they are unlikely to explain all the differences between the standard 1-D model and WACCM6. Because temperature changes with time and space in 3-D models, more work is needed to understand the role of temperature in affecting the mean ozone column depth.

Another important parameter in the 1-D model is the eddy diffusion coefficient, K, which is derived from empirical studies [32–34]. See the solid blue curve in figure 2*b*. Although theory cannot predict the exact magnitude of K, it provides some guidance on how K might change at lower $pO_2$. A decrease in $pO_2$ causes a decrease in stratospheric ozone and a corresponding decrease in stratospheric temperature. By reducing or eliminating the stratospheric temperature inversion, this could plausibly increase vertical transport in the lower stratosphere. To determine whether this would affect the ozone column depth in the 1-D model, we increased K in this region (see dashed and dashed-dotted curve in figure 2*b*) and reran the 1-D model. Surprisingly (to us), the ozone column depth actually increased at the higher $O_2$ levels (1 and 0.1 PAL) (table 1). That is because the increase in ozone in the troposphere outweighed the decrease in ozone in the stratosphere. At lower $O_2$ levels, though, the change in eddy diffusion coefficients had almost no effect on ozone column depth, because the ozone layer had already moved down to the lower stratosphere/upper troposphere. Thus, a change in vertical transport rates seems unlikely to explain the difference between column depths calculated by WACCM6 and by the 1-D model at low $pO_2$. Nonetheless, 3-D models calculate vertical transport quite differently, so we cannot rule out this being a factor in the discrepancies between those models and our 1-D model.

## 3.1. Modern $O_2$ level

Let us look more closely at the differences in predicted ozone amounts. At 1 PAL $O_2$, all four models predict roughly the same column depth, approximately 300 DU. ('PAL' means 'times the present atmospheric level'. 'DU' stands for 'Dobson units'; 1000 DU = 1 atm cm.) Slight differences are observed (table 1): Segura *et al*. [3] predicted 311 DU; C22 [4] predicted 279 DU; Way *et al*. [6] and our new eight-Gauss-point, 1-D model both predict 298 DU. The standard 1-D result drops to 296 DU when chlorine chemistry is included. The eight-Gauss-point model is a revised version of the Segura *et al*. [3] model and is described further below and more in the electronic supplementary material. It is represented by the green curves in figure 1. For comparison, the World Ozone and UV Radiation Data Center (WOUDC) reported a global average ozone column depth of approximately 292 DU for 1980 [35], but it should be noted that the C22 [4] calculation is for the pre-industrial atmosphere, not the modern atmosphere. The reported WOUDC value decreased by a little over 4% between 1980 and 1994 because of depletion by chlorine compounds and has since recovered.

Before trying to account for the differences between the 1-D and 3-D calculations, we should start by explaining the differences in the older and newer 1-D calculations from the Kasting group. The Segura *et al*. [3] model assumed a diurnal averaging factor of 0.5, i.e. the photolysis rates were multiplied by this fraction. The solar zenith angle was then adjusted to 45° to give approximately the 'right' ozone column depth for the modern atmosphere. The modern globally averaged ozone column depth was taken from McClatchey *et al*. [36], who listed it as 320 DU. Segura *et al*. calculated 311 DU, so they were still a little on the low side, despite their relatively low solar zenith angle. The Segura *et al*. methodology overestimated the globally averaged solar UV flux by approximately 40% (= cos 45°/cos 60°). Adopting a solar zenith angle of 60° would give the right solar UV flux but would cause the model to severely underestimate the globally averaged ozone column depth.

One strategy for dealing with this issue in a 1-D model is to use the insolation-averaged daytime solar zenith angle of 48.2° suggested by Cronin [37]. Combining this with a diurnal averaging factor of 0.375, or 3/8, gives the right globally averaged solar flux, along with a reasonable ozone column depth of 268 DU. We used that strategy in a recent paper by Liu *et al*. [7]. That number is consistent with the revised lower estimate of ozone column depth based on observations. Here, we go a step further and use an eight-point Gaussian integration over the sunlit hemisphere (see electronic supplementary material). This procedure places some weight on calculations at very low solar zenith angles (Sun high in the sky) that allow more photons to reach the lower stratosphere and, thus, increase the column-integrated $O_2$ photolysis rate. This creates more ozone compared with the 48.2° model, bringing it closer to the WOUDC value.

Our present 1-D model and the one used by Segura *et al*. [3] differ in at least two more important ways:

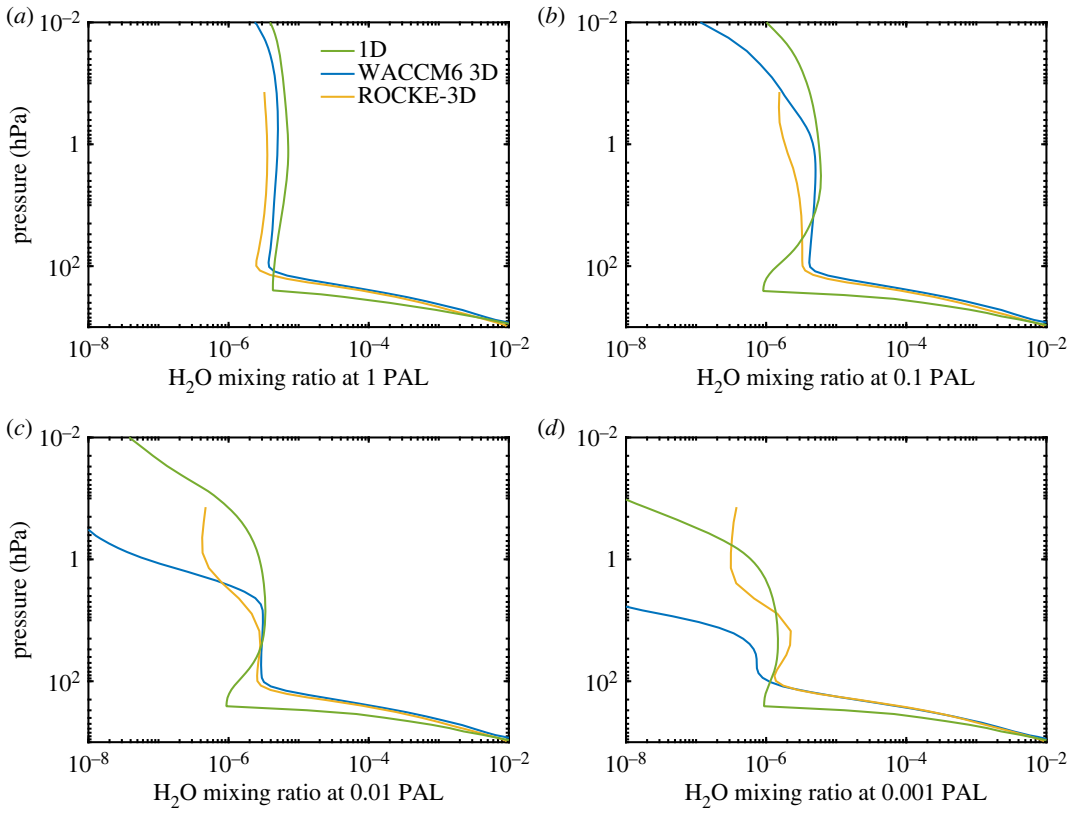


**Figure 3.** $H_2O$ mixing ratio at different values of $pO_2$ in the 1-D (green curve), WACCM6 3D (blue curve) and ROCKE-3D (yellow curve) models.

1) The Segura *et al*. model included chlorine chemistry, whereas our 'standard' 1-D model does not. But, as noted earlier, we added chlorine chemistry back into the model for some of the calculations done later during this study. The assumed source of chlorine in the Segura *et al*. model was 0.5 ppbv of methyl chloride, $CH_3Cl$, near the surface, supported by a flux of 7.29 Tg($CH_3Cl$) $yr^{-1}$. (This flux drops to 3.91 Tg($CH_3Cl$) $yr^{-1}$ in the standard model with chlorine discussed here, because of the change in how photolysis rates are calculated). (Recall that the Segura *et al*. model had too many solar UV photons.) The methyl chloride *flux* was held constant in calculations at lower $O_2$ levels. We return to the question of lower boundary conditions in §5.1 because the predicted concentrations of other biogenic species (e.g. $CH_4$ and $N_2O$) also depend critically on this parameter.
2) Our new model assumes less $H_2O$ in the upper troposphere than did the model of Segura *et al*. [3]. Segura *et al*. used a tropospheric relative humidity (RH) profile from Manabe & Wetherald [38]. That model yields approximately 6 ppmv at the tropopause cold trap, considerably higher than the values seen in the two 3-D models with which we compare. (The tropopause is set at 10 km, or approximately 300 mbar, in the 1-D model.) So, in the new model we modified the RH profile to produce approximately 4 ppmv $H_2O$ at the tropopause. By comparison, the ROCKE-3D model has about 2 ppmv $H_2O$ in the lower stratosphere, and the WACCM6 3D model has approximately 3 ppmv $H_2O$ (figure 3*a*). The 3-D models have a cold, high equatorial tropopause that effectively vacuums water vapour out of the stratosphere. The $H_2O$ concentration increases with altitude in the stratosphere in all three models as a result of methane oxidation. By comparing the ozone column depth in the high-$H_2O$ version of the 1-D model (287 DU, case 9 in table 1) with that in our standard 1-D model (298 DU, case 1 in table 1), it can be seen that the high-$H_2O$ model results in roughly a 3% (21 DU) decrease in ozone column depth at 1 PAL $O_2$. More details are provided in §1.1.2 in electronic supplementary material.

## 3.2. Lower $O_2$ levels

While the three models agree fairly well on the ozone column depth of the present atmosphere, the predictions of the WACCM6 model diverges from the other two models at low $pO_2$. For example, the

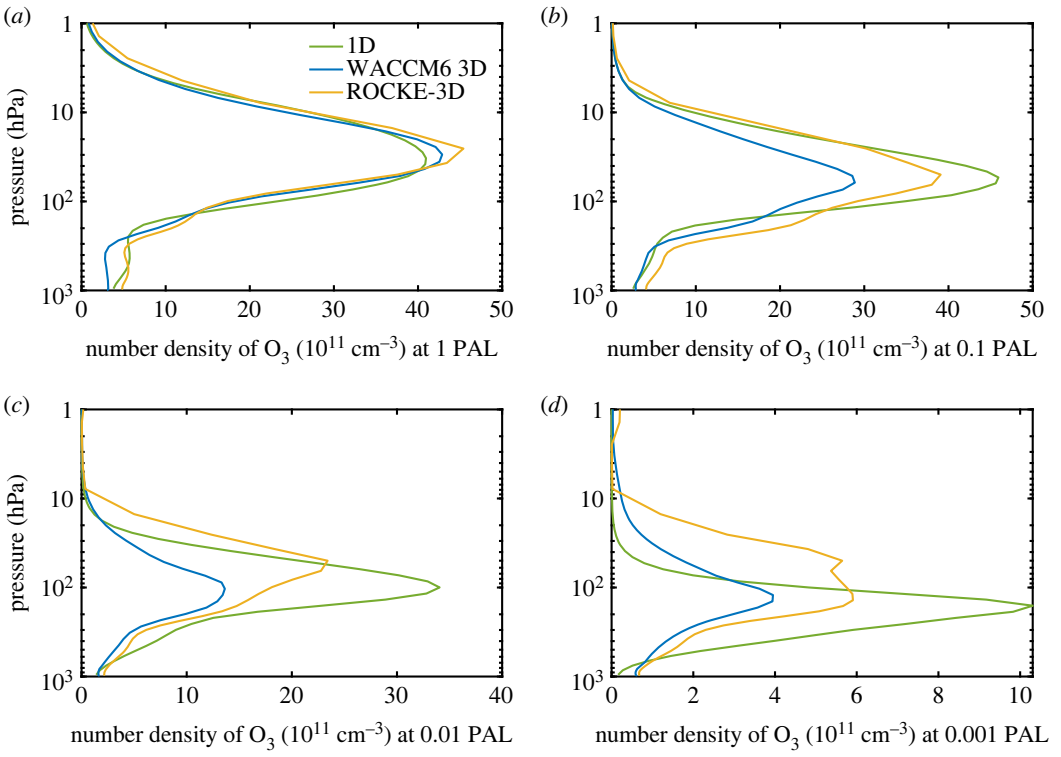


**Figure 4.** Comparison of ozone number density at different values of $pO_2$ in the 1-D (green curve), WACCM6 3D (blue curve) and ROCKE-3D (yellow curve) models.

discrepancy between WACCM6 and the standard 1-D model is already a factor of 1.5 at 0.1 PAL $O_2$ and rises to 2.2 below that $O_2$ level (figure 1 and table 1). The column depth in the 1-D model is consistently higher than WACCM6 at low $pO_2$. ROCKE-3D remains close to the 1-D model down to $10^{-3}$ PAL but predicts only half as much ozone below that. (WACCM6 does not have a calculation at $10^{-4}$ PAL $O_2$.) The Jaziri *et al*. [5] 1-D model column densities agree with WACCM6 at $10^{-3}$ PAL, while the 3-D model columns are about a factor of 2 less. At $10^{-4}$ PAL both of these simulations are less than the 1-D model values. Note that when chlorine chemistry is included, the new 1-D model predicts ozone column depths that are close to those calculated by Segura *et al*. [3]. This is somewhat surprising, given the lower (and more correct) UV fluxes calculated in the newer model. But it may simply show that the calculation is relatively insensitive to the solar UV flux, because $O_2$ and $H_2O$ photolyse at roughly the same wavelengths. To look more closely at where these discrepancies arise, we compare vertical profiles of ozone number density at different $pO_2$ levels (figure 4). Ozone is shown on a linear scale to highlight the differences in the stratosphere, where most of the ozone is found. At low $pO_2$, the peak number density of ozone in the 1-D model is always larger than that in the two 3-D models, and the WACCM6 model always shows the smallest peak number density. For example, the peak ozone density in the WACCM6 model is approximately $1.4 \times 10^{12}$ cm$^{-3}$ at 0.01 PAL and approximately $4 \times 10^{11}$ cm$^{-3}$ at 0.001 PAL, which is less than half that predicted by the 1-D model for those $O_2$ levels (figure 4*c*,*d*). At low $pO_2$, the ozone layer is also more strongly peaked in the 1-D model than in either 3-D model.

Note also that the peak ozone density occurs lower in the atmosphere as the $O_2$ concentration decreases. (This is not a new result: it was pointed out 50 years ago by Ratner & Walker [39].) The ozone layer migrates downward as $pO_2$ decreases because solar UV radiation capable of dissociating $O_2$ penetrates more deeply into the atmosphere. By the time $pO_2$ has decreased to $10^{-3}$ PAL, the peak ozone density in the 1-D model has moved down to approximately 200 mbar (12 km)—a region that is much drier in the 1-D model than in the two 3-D models (figure 3*b*–*d*). Lower $H_2O$ in this region implies lower $HO_x$ production, and that in turn should imply less destruction of $O_3$. The two

important reaction sequences are

$$O_3 + h\nu \rightarrow O_2 + O(^1D), \tag{3.1}$$

$$O(^1D) + H_2O \rightarrow 2OH \tag{3.2}$$

and

$$H_2O + h\nu \rightarrow OH + H. \tag{3.3}$$

Reactions (3.1) and (3.2) dominate OH production in the modern atmosphere, but reaction (3.3) becomes important at low $pO_2$ (see §4). We suspect that some of the differences between the 1-D model and WACCM6 may arise from differences in upper tropospheric $H_2O$ concentrations. Indeed, comparison of Case 1 and Case 9 in table 1 shows that the high-$H_2O$ version of the 1-D model has 27% less ozone than the standard model at 0.001 PAL $O_2$. So, this is a big effect. But $HO_x$ production also depends on $H_2O$ photolysis rates, which are affected by shielding of $H_2O$ by $O_2$ and $O_3$. $O_2$ photolysis is particularly critical and is calculated differently in each model. We examine these factors more closely in the next section.

Before doing that, though, we should mention the two black curves in figure 1*a*,*b*. These show calculations by Jaziri *et al*. [5], in which they compared ozone column depths calculated with a 3-D model and a 1-D model that share the same photochemical scheme. This paper, which came out too recently to be included in the present intercomparison, was focused on a different problem, namely, the transition from anoxic to oxic conditions, sometimes called the Great Oxidation Event (GOE). Their calculations were performed for $O_2$ mixing ratios of $10^{-3}$ or below ($pO_2 \leq 0.005$ PAL), so they overlap with the other models only at the lowest $O_2$ levels studied here. They also included 100 ppmv of $CH_4$, omitted halogen and nitrogen chemistry, and did not include gravity waves, which contribute to the forcing of the Brewer–Dobson circulation. Thus, their calculations are not directly comparable to the models discussed here, but inclusion of these processes would probably reduce the ozone column amounts they report. Their calculations show something that may very well be significant: the ozone column depths calculated by their 3-D model were always significantly lower than those found in their 1-D model (we show their 1-D calculation with a solar zenith angle of 40°, which is close to the 45° zenith angle used by Segura *et al*. [3]). This suggests that 1-D calculations are missing some fundamental process that tends to reduce ozone levels at low $pO_2$, supporting the argument made in C22 [4]. We return to this point in §5.2.

# 4. Photolysis rates of $H_2O$ and $O_2$

## 4.1. Validation of the 1-D model at 1 PAL $O_2$

Before attempting to compare $O_2$ photolysis rates in the three photochemical models, we should first ask: do any of them agree with the most up-to-date calculations of $O_2$ photolysis rates? As discussed further below, the difficult part of this calculation is to estimate absorption in the $O_2$ Schumann–Runge bands between 175 and 205 nm. An accurate line-by-line calculation of $O_2$ photolysis rates in the modern atmosphere was performed by Fernández *et al*. [40] using data from the HITRAN database (https://hitran.org/). This calculation was done for the present $O_2$ level using the 1976 US Mid-latitude Standard Atmosphere temperature profile. The same modern temperature profile is used in the 1-D model (figure 2*a*). Photolysis rates of $O_2$ from that model and from Fernández *et al*. were computed at 0°, 60° and 80° solar zenith angles (figure 5). These calculations were done for the dayside, i.e. they did not include diurnal averaging. Photolysis rates calculated by the two models are in reasonably good agreement at all altitudes except near the very top of the atmosphere, where Fernández *et al*. compute higher rates. (This does not matter much for ozone column depth because most of the ozone is found at lower altitudes.) What look like small differences on the log scale used in figure 5 can actually be quite significant, though. At a solar zenith angle of 0° and an altitude of 40 km, for example, the photolysis rate predicted by our 1-D model is higher than that found by Fernández *et al*. by approximately 25%. This difference occurs near where odd oxygen ($O_x$) production peaks and may account for the differences in $O_x$ production between the 1-D model and WACCM6 (see next section).

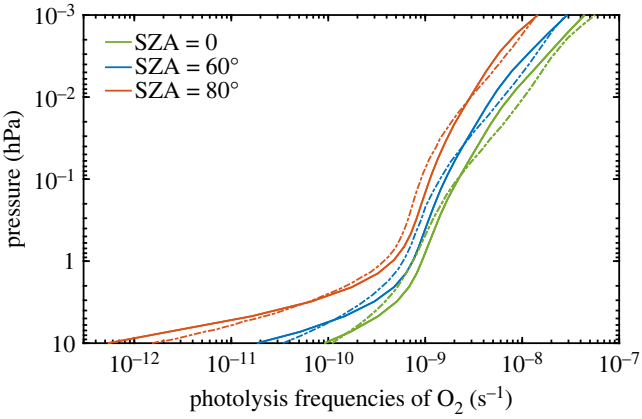


**Figure 5.** Comparison of photolysis frequencies of $O_2$ for the modern atmosphere in the Kasting group 1-D model (solid curves) and from the model of Fernández *et al*. [40] (dashed curves). SZA, solar zenith angle.

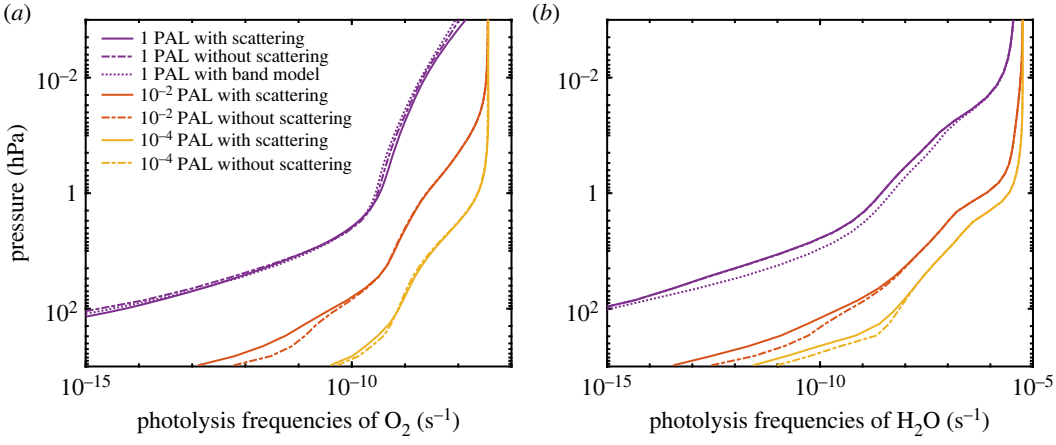


**Figure 6.** Photolysis frequencies of $O_2$ (*a*) and $H_2O$ (*b*) calculated in the 1-D model with and without scattering at three different $O_2$ levels.

## 4.2. Photolysis of $O_2$ in the Schumann–Runge bands

As already mentioned, photolysis of $O_2$ in the SR bands plays a key role in these calculations. The 1-D model uses an exponential sum formulation for the $O_2$ absorption coefficient which allows that model to include multiple scattering. The exponential sums in the 1-D model were derived more than three decades ago by fitting the Allen & Frederick [22] band model at 1 PAL $O_2$ (see electronic supplementary material). As a first step towards testing this parametrization at lower $pO_2$, we show calculated $O_2$ photolysis frequencies versus altitude for three different atmospheric $O_2$ levels in figure 6*a*. Calculations were performed using the exponential sum formulation, both with (solid curves) and without (dashed curves) scattering. When scattering is neglected at 1 PAL $O_2$, the photolysis rates of $O_2$ and $H_2O$ are almost unaffected, as expected. Note also that the no-scattering calculation agrees well with the original Allen and Frederick band model at 1 PAL $O_2$, as it should. Significant differences arise at low-$O_2$ levels, however. At 0.01 PAL $O_2$, the photolysis rate of $O_2$ at the surface is five times higher when scattering is neglected, and the photolysis rate of $H_2O$ is higher by a factor of 8. The reason is that the effective path length of the incoming photons is significantly increased when multiple scattering is included. So, it is clear that multiple scattering at SRB wavelengths should be included when performing these low-$O_2$ calculations. But one should also realize that the exponential sum coefficients calculated at 1 PAL $O_2$ may not be accurate at lower $pO_2$ because the temperatures and pressures in the region where SR absorption occurs can be quite different. So, even the 1-D parametrization with scattering is less than ideal. We explain how this problem can be corrected in §6.

The WACCM6 3-D model used by C22 [4] parametrizes absorption/photodissociation in the $O_2$ SR bands using a method developed by Koppers & Murtagh [20] and Marsh *et al*. [41]. This method does not include scattering within the SR bands. For 1 PAL $O_2$ conditions, scattering in the SR bands is not

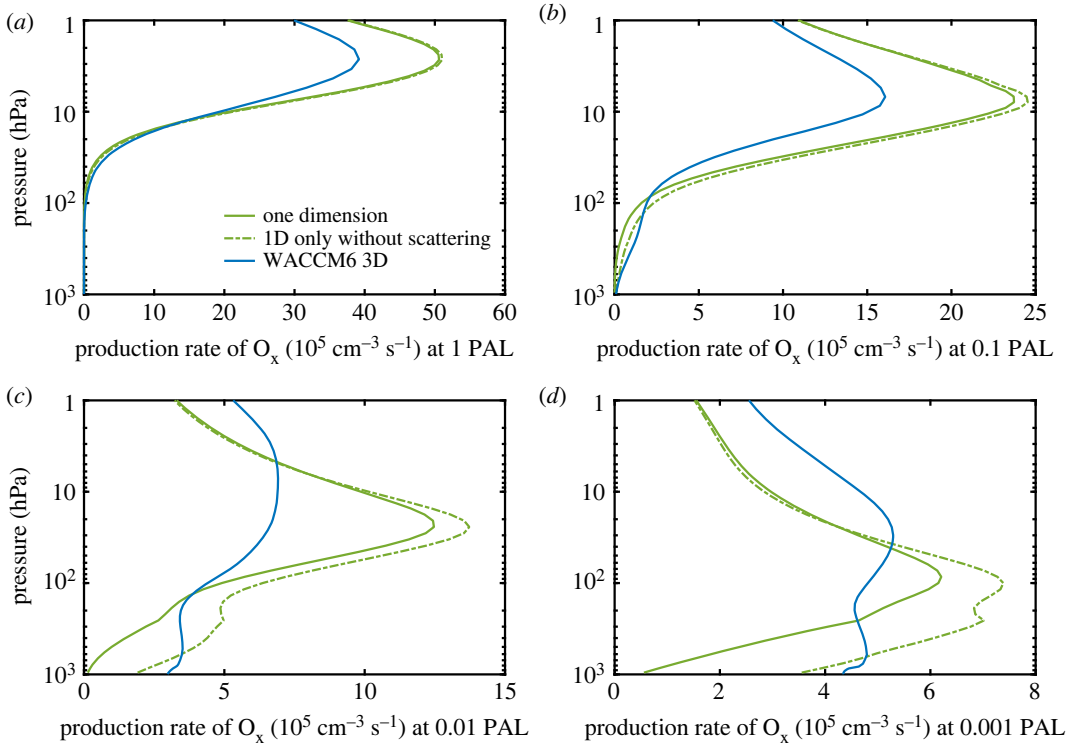


**Figure 7.** Production rate of odd oxygen ($O_x$) at different values of $pO_2$ in the standard 1-D model (solid green curve), the standard 1-D model without scattering (dotted-dashed green curve) and the WACCM6 3-D model (globally averaged, solid blue curve).

important and the parametrization used in WACCM6 agrees well with the line-by-line calculations. The implementation of this algorithm in the WACCM6 model previously neglected absorption of SR-band radiation by $H_2O$ and $CO_2$. That is a separate issue that will be discussed in the next section. Neglecting scattering is a valid approximation in the present atmosphere because most solar radiation at these wavelengths is absorbed above 60 km, where the air is thin. But at 0.01 PAL $O_2$, the relative importance of Rayleigh scattering (most of which is done by $N_2$) should be higher by a factor of 100 compared with today because solar UV radiation will penetrate deeper into the atmosphere. Thus, scattering at SRB wavelengths should be included when performing calculations at low $pO_2$.

## 4.3. Comparison of photolysis rates in the 1-D and 3-D models

Comparisons of globally averaged $O_2$ and $H_2O$ photolysis frequencies (in units of $s^{-1}$) calculated by the 1-D model and by WACCM6 are shown in electronic supplementary material, figure S5. Here we show in figure 7 the globally averaged odd-oxygen production rate (in units of $cm^{-3}$ $s^{-1}$) as a function of pressure, which highlights fundamental differences between the 1-D model and the WACCM6 3-D model. The standard 1-D model predicts higher (and more strongly peaked) $O_2$ photolysis rates than does WACCM at 0.1 and 0.01 PAL $O_2$. At 1 and 0.1 PAL $O_2$, the odd oxygen production rate around 3 mbar $hPa^{-1}$ (approx. 40 km) is about 25% higher in the 1-D model than in the 3-D model. At 0.01 and 0.001 PAL $O_2$, $O_x$ production is almost twice as high in the 1-D model and is much more strongly peaked. As mentioned earlier in §4.1, the difference in $O_2$ photolysis rates between the 1-D model and Fernández *et al*. line-by-line calculation is about 25% at approximately 40 km in the modern atmosphere. This may explain, at least partly, the 25% difference for $O_2$ photolysis rate between the 1-D model and WACCM6 3-D model at higher $O_2$ levels. To say this differently, for the modern atmosphere the $O_2$ photolysis rates from WACCM6 agree with Fernández *et al*. [40] better than those computed by the 1-D model, probably because WACCM6 uses a more up-to-date parametrization of the SR bands (see next section). We also show in electronic supplementary material, table S2 that applying WCCM6 UV fluxes, which are lower than that in the SR bands in the 1-D model, leads to an approximately 10% reduction in total column-integrated $O_2$ photolysis rate at 0.01 PAL, but still cannot explain the large proportion of the discrepancies in the ozone column depth.

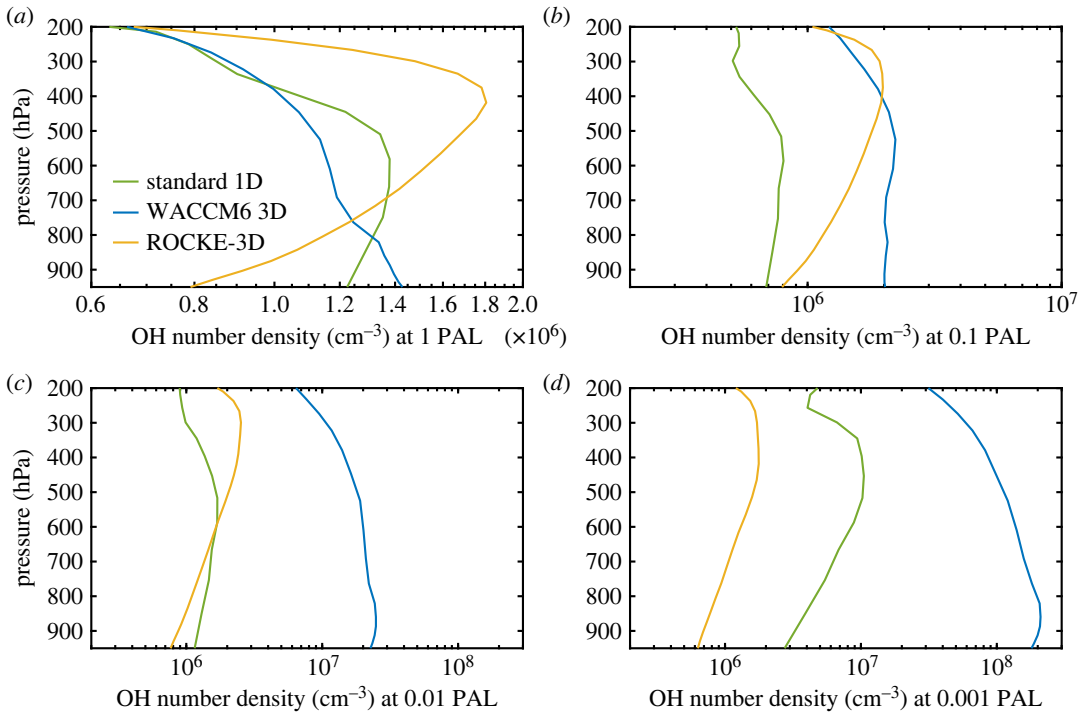


**Figure 8.** OH number density as a function of $pO_2$ in standard 1-D (green curve), WACCM6 3D (blue curve) and ROCKE-3D (yellow curve) models.

## 4.4. OH concentrations at low-$O_2$ levels

Photolysis of $H_2O$ is particularly important at low $pO_2$ because it leads to production of OH, which is the most important oxidant in both the modern and ancient troposphere. As shown in figure 8, tropospheric OH concentrations are very different in the three models at some $O_2$ levels. Figure 8*a* shows comparisons at 1 PAL of $O_2$. The 1-D model predicts an OH number density, $n_{OH}$, of $1.25 \times 10^6$ cm$^{-3}$ at the surface. The $n_{OH}$ from WACCM6 is about 15% higher; $n_{OH}$ from ROCKE-3D is about 30% lower. Peak tropospheric OH densities occur at 600 hPa (approx. 4 km) in the 1-D model (approx. $1.4 \times 10^6$ cm$^{-3}$), 400 hPa (approx. 7 km) in ROCKE-3D (approx. $1.8 \times 10^6$ cm$^{-3}$), and at the surface in WACCM6 (approx. $1.45 \times 10^6$ cm$^{-3}$). As a comparison, the standard reference of annually and globally averaged OH concentration peaks around $1.5 \times 10^6$ cm$^{-3}$ at 700 hPa in Spivakovsky *et al*. [42] (see their fig. 8). The reason for these discrepancies is probably due to the different treatments of the absorption by $H_2O$ and $CO_2$ within the SR bands, and we cannot rule out other factors that may be related to the spatial inhomogeneity of OH, including the cloud distribution in the 3-D models. The 1-D model atmosphere is cloud-free. Also note that the OH profiles in the WACCM6 3D simulations differ from those in Spivakovky *et al*. [42] because WACCM6 used here assumes a pre-industrial atmosphere without pollutants.

At low $pO_2$, the discrepancies in OH density are much larger. We focus here on the most extreme case: surface OH densities at 0.001 PAL $O_2$. As shown in figure 8*b*, the 1-D model predicts $n_{OH} = 3 \times 10^6$ cm$^{-3}$, ROCKE-3D predicts $2.2 \times 10^5$ cm$^{-3}$ (14 times lower than the 1-D model), and WACCM6 predicts $2 \times 10^8$ cm$^{-3}$ (almost 70 times higher than the 1-D model). The low surface OH number densities predicted by ROCKE-3D are easily explained, as this model does not include $H_2O$ photolysis at SR-band wavelengths (reaction (3.3) in §3.2). $H_2O$ photolysis is a major source of tropospheric OH at low $pO_2$ (figure 9). The disagreement between WACCM6 and the 1-D model can be explained in a similar manner. At high $pO_2$, tropospheric OH is produced mostly by reaction (3.2) (§3.2), but at low $pO_2$, reaction (3.3) becomes important. The standard 1-D model, which was designed for low-$O_2$ levels, handles this transition self-consistently. But WACCM6, which was designed for the modern atmosphere, does not. As pointed out in the previous subsection, WACCM6 neglects scattering within the wavelength region of the SR bands, and it does not treat either $H_2O$ or $CO_2$ as major absorbers of solar UV radiation in C22 [4]. (It allows these species to photolyse, but it does not consider their effect on the UV opacity.) The latter assumption is acceptable for the modern atmosphere because $CO_2$ is scarce and because radiation at these wavelengths is absorbed high in the atmosphere where $H_2O$ is

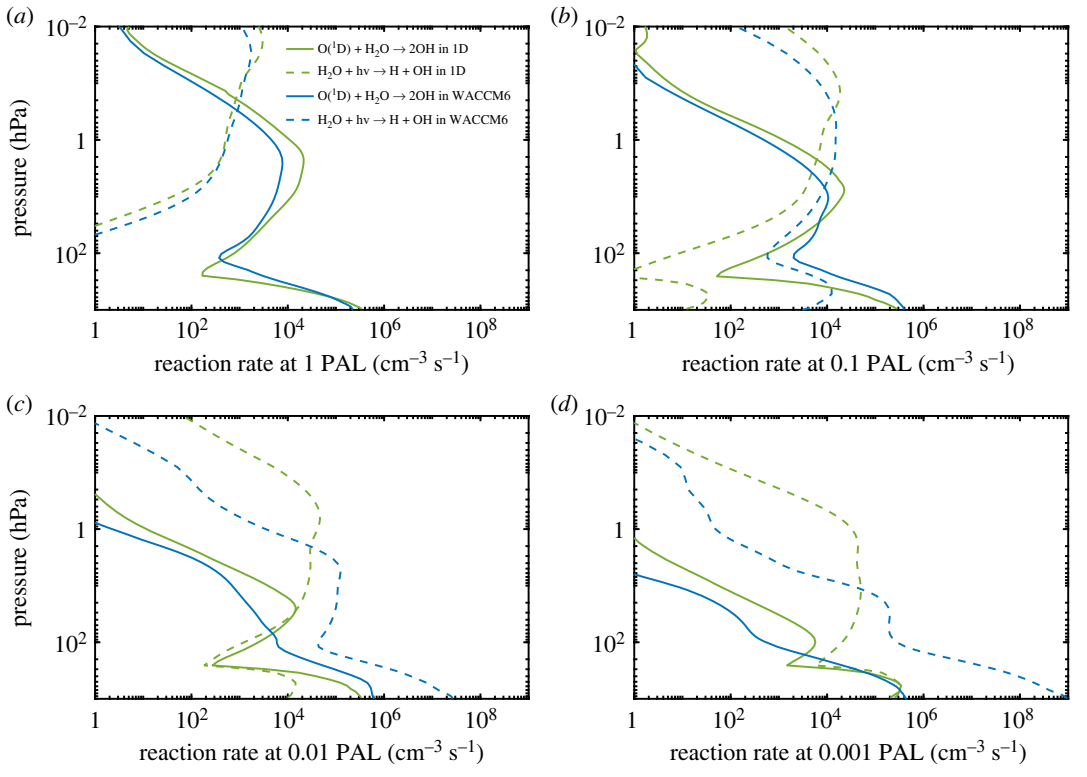


**Figure 9.** OH production from the reaction of O ($^1$D) with $H_2O$ and from photolysis of $H_2O$ at different $O_2$ levels in the 1-D and WACCM6 3-D models.

even scarcer. At 0.001 PAL $O_2$, however, $CO_2$ is 50% more abundant than $O_2$ (assuming modern $CO_2$ levels), and SR-wavelength radiation penetrates to the lowest atmospheric layer where $H_2O$ is more than 50 times as abundant as $O_2$.

To test the impact of omitting these factors, we eliminated scattering between 175 and 250 nm in the 1-D model and treated $H_2O$ and $CO_2$ as minor absorbers within this same wavelength region. The results are shown in figure 10. At 0.001 PAL, OH production near the surface increases by more than a factor of 1000 compared with our standard 1-D simulation, yielding almost as much OH production as seen in WACCM6 model (figure 10*d*). This comparison explains why tropospheric OH concentrations are so much higher in WACCM6. These calculations were run for only one time step, so that they started from the same background atmosphere. By running the 1-D model to convergence, we can look more closely at how the OH number density would change when scattering and absorbers are neglected at 0.001 PAL. The result is shown in figure 11. The OH number density near the surface increases by more than a factor of 200. We also tested only the scattering effect at two different wavelength ranges: SR bands (175–205 nm) and Herzberg continuum (205–250 nm) because WACCM6 does have scattering between 200 and 250 nm. We found that OH production at low $pO_2$ is mainly affected by the treatment of the SR bands, and whether we include scattering within the Herzberg continuum does not make a measurable difference.

The effect of $H_2O/CO_2$ absorption on OH production and thus its concentration is also noticeable in WACCM6 after adding the absorption. For example, at 0.001 PAL, the new simulation in WACCM6 including $H_2O/CO_2$ absorption predicts OH production near the surface will decrease to almost the same level as in the 1-D model (figure 10*d*). This also leads to a decrease by more than a factor of 200 in OH number density in the new WACCM6 simulation at 0.001 PAL (figure 11*d*). So, this discrepancy can be considered resolved.

## 5. Why predicted ozone column depths and methane lifetimes differ at low-$O_2$ levels

We are now in a somewhat better position to understand why the ozone column depths and methane lifetimes predicted by the 1-D and 3-D models differ at low-$O_2$ levels. Both issues are at least partly

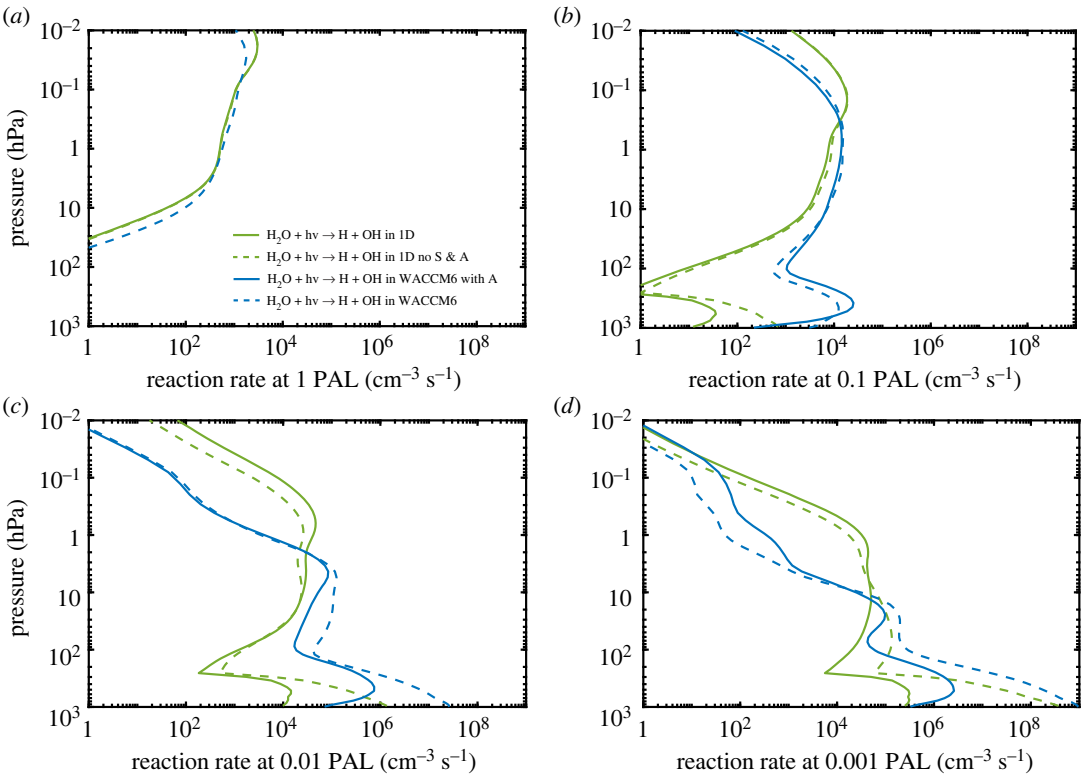


**Figure 10.** Comparisons of the rate of $H_2O$ photolysis at different $O_2$ levels in the 1-D (green curves) and WACCM6 3-D (blue curves) models. The solid green curve shows the standard run in the 1-D model, and dashed green curve shows the same run without scattering and without treating $CO_2$ and $H_2O$ as major absorbers at SR wavelengths (no S & A). The solid blue curve shows the WACCM6 simulation with absorption by $H_2O$ and $CO_2$, and the dashed blue curve shows the WACCM6 simulation without absorption by $H_2O$ and $CO_2$.

related to tropospheric OH concentrations. We start with the methane lifetime question, as that discrepancy is now fully understood.

## 5.1. Methane lifetimes at low-$O_2$ levels

In addition to predicting lower ozone column depths at low $pO_2$, C22 also predicted that methane should have a much shorter lifetime than predicted in previous 1-D modelling efforts. C22 [4] suggested that these two phenomena were closely related: the lower ozone column depths allowed more solar UV radiation to penetrate to the troposphere, creating more $O(^1D)$ from ozone photolysis (reaction (3.1)), and thereby increasing OH concentrations and lowering the lifetime of $CH_4$. The two major photochemical loss processes for methane in the modern atmosphere are the reactions

$$CH_4 + OH \rightarrow CH_3 + H_2O, \tag{5.1}$$

and

$$CH_4 + O(^1D) \rightarrow CH_3 + OH. \tag{5.2}$$

These reactions remain the dominant loss processes for methane at all $O_2$ levels studied here. Methane can also be photolysed directly, but this reaction happens only at very short wavelengths (less than 145 nm) and thus occurs high up in the atmosphere, even at low $pO_2$.

Because methane is not produced within the atmosphere, methane lifetimes in all three models can be calculated by dividing the $CH_4$ column depth by the $CH_4$ input flux at the surface, or by integrating the total loss rate across the whole atmosphere when the mixing ratio is fixed. ('Surface' methane lifetimes shown in table 2 of C22 [4] are not used for this comparison because such a calculation considers only $CH_4$ loss in the lowermost atmospheric layer.) Because methane is well-mixed in the lower atmosphere at all $O_2$ levels, the methane column depth can be approximated as the $CH_4$ number density in the bottommost layer times the atmospheric scale height (about 7.5 km).

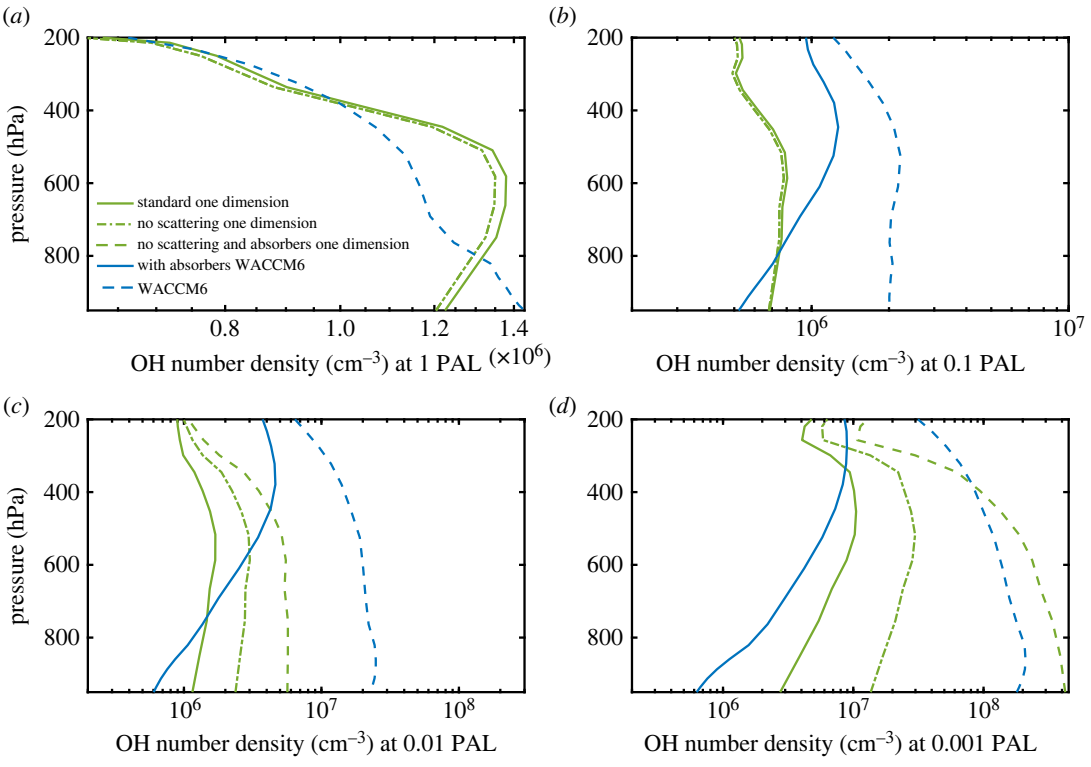


**Figure 11.** OH number density as a function of $pO_2$ in the standard 1-D model (green curves) and the WACCM6 model (blue curves). In the 1-D model, solid green curves represent results from the standard runs, dashed green curves represent results without scattering and absorption by $H_2O$ and $CO_2$ between 175 and 250 nm, and dashed-dotted green curves show the simulation without scattering in this same wavelength region. In the WACCM6 model, solid blue curves represent results with absorption by $H_2O$ and $CO_2$ between 175 and 205 nm, and dashed blue curves represent results without absorption by $H_2O$ and $CO_2$ in this wavelength region.

Comparisons of methane concentrations and lifetimes between the 1-D model and WACCM6 model are shown in figure 12. The 1-D model calculations were done by fixing the surface $CH_4$ mixing ratio at its (approximate) modern value, 1.6 ppmv, at 1 PAL $O_2$. The model then calculates the $CH_4$ flux ($1.13 \times 10^{11}$ cm$^{-2}$ s$^{-1}$) needed to support it. In geochemists' units, this is equivalent to a flux of 480 Tg($CH_4$) yr$^{-1}$. This yields a $CH_4$ lifetime of 8.0 years for the modern atmosphere, which is close to the accepted value in Kirschke *et al*. [43]. At lower $O_2$ levels, the $CH_4$ flux was held constant, and the model calculated its surface mixing ratio (figure 12*a*). The $CH_4$ mixing ratio—and, thus, its lifetime—peaks at 0.1 PAL $O_2$. This peak appears to be caused by lightning. In today's atmosphere, lightning is the major non-anthropogenic source of nitrogen oxides in the troposphere via the high-temperature reaction: $N_2 + O_2 \leftrightarrow 2NO$. The 1-D model scales the column-integrated rate of NO production to lower $O_2$ levels by assuming thermodynamic equilibrium at a 'freeze-out' temperature of 3500 K in the expanding, cooling, cylindrical shock wave surrounding the lightning bolt. As $O_2$ drops to 0.1 PAL, the NO production rate decreases to just one-third of that for today, based on this parametrization. According to models of smog chemistry, NO reacts with the by-products of methane (or higher hydrocarbon) oxidation to produce $O_3$, and this, in turn, leads to more OH through reactions (3.1) and (3.2). Thus, at 0.1 PAL $O_2$, less NO leads to less $O_3$, less OH and a longer methane lifetime. As $O_2$ continues dropping below this level, more OH is produced by reaction (3.3), which leads to a decrease of $CH_4$ lifetime. The $CH_4$ mixing ratio falls to approximately 0.1 ppmv at $10^{-4}$ PAL $O_2$, and its lifetime decreases to about eight months. The changes in tropospheric $O_3$ caused by this mechanism are too small to account for the discrepancies in ozone column depth.

The WACCM6 model described in C22 [4] was operated in two different modes. One set of calculations was done in a similar manner as the 1-D calculations, except that the standard calculation was done for the pre-industrial atmosphere (0.8 ppmv $CH_4$). This yielded a surface $CH_4$ flux of $5.6 \times 10^{10}$ cm$^{-2}$ s$^{-1}$ (approx. 240 Tg($CH_4$) yr$^{-1}$), which corresponds to a $CH_4$ lifetime of 9 yr. Fixed fluxes of 50, 500 (present level), and 5000 Tg($CH_4$) yr$^{-1}$ were then used as the lower boundary condition for $CH_4$ in calculations done at 0.1 and 0.01 PAL $O_2$. (The 0.1 PAL run was done subsequent to the

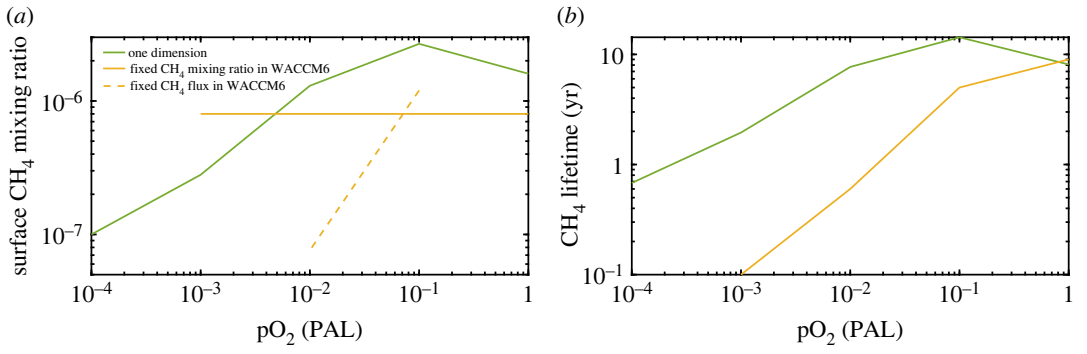


**Figure 12.** Surface $CH_4$ mixing ratio (*a*) and $CH_4$ lifetime (*b*) at different $pO_2$ levels in the 1-D (solid green curve), WACCM6 3-D (yellow curve) models. The solid yellow curve in (*a*) shows fixed $CH_4$ mixing ratio (0.8 ppmv) runs in WACCM6, whereas the dashed yellow curve shows fixed $CH_4$ flux (500 Tg $yr^{-1}$) runs. The WACCM6 methane lifetimes in (*b*) were calculated from the fixed mixing ratio runs.

publication of C22 [4].) Results for the 500 Tg($CH_4$) $yr^{-1}$ run are shown in figure 12*a*. In another set of WACCM6 calculations, the $CH_4$ mixing ratio was held fixed at 0.8 ppmv at all $O_2$ levels (figure 12*b*). In these simulations, the $CH_4$ lifetime dropped to as low at 0.1 yr at 0.001 PAL $O_2$. Thus, a very large $CH_4$ flux (approx. 80 times the present value) would have been needed to sustain such a mixing ratio if this calculation was correct. But we showed in the previous section that tropospheric OH concentrations at 0.001 PAL may be overestimated by a factor of 200 in the WACCM6 model because of the treatment of $O_2/H_2O$ photolysis. So, these calculated lifetimes could be as much as 200 times too low at 0.001 PAL. In addition, the total $NO_x$ production from lightning in the C22 [4] does not scale to lower $pO_2$; instead, it is almost constant for each $O_2$ level (see details in electronic supplementary material). This higher NO compared with the 1-D model at 0.1 PAL could result in more $O_3$, and thus more OH. Therefore, shorter $CH_4$ lifetime would be expected as C22 [4]. But the lightning effect at much lower $pO_2$ (less than 0.1 PAL) on $CH_4$ lifetimes is not expected to be solved in this paper. The actual underestimation of the methane lifetime is probably smaller than this because the discrepancies in calculated OH abundances decrease with altitude.

As an aside, another biogenic trace gas, $N_2O$, was also treated with fixed mixing ratio (270 ppbv) lower boundary conditions in the WACCM6 model. This also results in high surface fluxes at low $pO_2$. At $10^{-4}$ PAL $O_2$, for example, the 1-D model calculates an $N_2O$ surface mixing ratio of approximately 0.8 ppbv, about 0.3% of the present value. Hence, keeping $N_2O$ fixed at 300 ppbv in the 1-D model would require a surface flux more than 300 times higher than today. This assumption is unlikely to account for the lower ozone column depths found by WACCM6, however, because at low $pO_2$ most $N_2O$ photolyses back to $N_2 + O$ rather than reacting with $O(^1D)$ to produce NO.

## 5.2. Ozone column depths at low $pO_2$

Although the reason(s) for the lower ozone column depths at low $pO_2$ in the WACCM6 model are not fully resolved, we do understand at least some of the issues. We number these below, for clarity:

1) Lower boundary conditions and chlorine chemistry clearly affect the calculated ozone column depths. We have done several sensitivity analyses on chlorine in both the 1-D and WACCM6 models. The results are listed in table 1 and details can be found in the electronic supplementary material. The 1-D model is extremely sensitive to the lower boundary condition on $CH_3Cl$, especially when scattering and absorption by $H_2O/CO_2$ is neglected at SR wavelengths (see cases 10 and 11 in table 1). In case 11, the ozone column depth decreases by a factor of 10 at 0.01 PAL $O_2$ when a fixed mixing ratio boundary condition is used for $CH_3Cl$. At 0.001 PAL $O_2$ ozone basically disappears and the code fails to converge. But the WACCM6 model appears to be much less sensitive to changes in lower boundary conditions (see cases 17–19 in table 1).
2) A second factor that clearly affects ozone column depths is upper tropospheric $H_2O$ densities. These are higher in WACCM6 than in the 1-D model because WACCM6 has a high tropical tropopause, allowing convection to bring $H_2O$ into the upper troposphere. Sensitivity experiments described in §§3.1 and 3.2 show that the 1-D model predicts less ozone when upper tropospheric $H_2O$ levels are increased. This effect is particularly pronounced at low $pO_2$, partly explaining why the 3-D

model predicts less ozone in these conditions. This may also help explain why the Jaziri *et al*. [5] 3-D model predicts less ozone than their 1-D model. But it does not explain why the same effect is not observed in the ROCKE-3D calculation.

3) The different parametrizations of $O_2$ photolysis in the SR bands cause $O_x$ production to be lower in WACCM6 than in the 1-D model. This issue can best be resolved by developing a more robust parametrization of absorption at these wavelengths (see §6).
4) Vertical transport is also very different in the two models. In the 1-D model, vertical transport is parametrized as eddy diffusion and is fixed at all $pO_2$ levels. By contrast, in WACCM6, as $O_2$ is decreased, the reduced levels of $O_3$ result in less stratospheric heating. Because the stratospheric polar vortex forms due to latitudinal temperature gradients, when $O_3$ is reduced, the average velocity of the polar vortex decreases. This change in wind fields seen in the WACCM6 simulations, including a weakened Brewer–Dobson circulation, is consistent with previous work [44,45] and affects the latitudinal distribution of $O_3$ (more details are included in the electronic supplementary material). The other 3-D models also have sophisticated vertical transport schemes, but the fact that they do not all agree shows that this problem is complicated.
5) Other factors that contribute to differences in calculated ozone column depths include: the temperature structure which modulates reactions rates and densities; chemical mechanism differences (e.g. assumed reaction rates, or the inclusion of heterogeneous chemistry on polar stratospheric clouds); and the inclusion of seasons and the diurnal cycle. While we believe these effects are small compared with the four factors discussed just above, future work should quantify their importance.

# 6. Suggestions for future research

As we have shown, a critical part of the photochemical schemes of all three models involves photolysis rates in the $O_2$ SR bands. None of the models compared here treats this problem rigorously. The Kasting *et al*. 1-D model may come closest because it includes multiple scattering at these wavelengths, but its limitations were pointed out earlier. A number of improved models of the SR bands have been published during the past 25 years [21,46–48]. These models presumably do an excellent job of parametrizing SR band absorption by $O_2$ in the modern atmosphere, but they may still not be optimal for low-$O_2$ atmospheres in which scattering is very important at these wavelengths. A widely used tool in calculating atmospheric absorption in the thermal-IR is that of correlated-k coefficients [49,50]. The Fernández *et al*. model, mentioned earlier, or some other line-by-line model, could be used to generate broadband, correlated-k coefficients for $O_2$ absorption that would remain valid for atmospheres containing variable amounts of $O_2$. Such coefficients, once generated, could then be used in both 1-D and 3-D photochemical models. We are pursuing this project with the Fernández *et al*. research group as this paper is being submitted.

We note that the excellent agreement between the ozone columns in the 1-D model and ROCKE-3D could be accidental. Photolysis of $O_2$ in ROCKE-3D does not cover the full SRB, or include absorption of UV radiation by $CO_2$ and $H_2O$, and yet the columns agree for the most part to within 3 DU. The lack of sensitivity of surface OH to the atmospheric $O_2$ level in ROCKE-3D is simply because ROCKE-3D does not include photolysis of $H_2O$ at SR band wavelengths.

Thinking more generally, it is important to perform intercomparisons among different types of models to help us better understand the palaeoatmosphere or the atmospheres of other Earth-like planets. Such intercomparisons are done routinely with complex climate models used to study the effects of anthropogenic warming. Very little work has been done to intercompare the types of models studied in this paper. An exception is the recent study by Harman *et al*. [51] in which three different low-$O_2$ photochemical models were compared to determine why some produced high abiotic $O_2$ levels whereas others did not. We hope to continue and expand the model intercomparison project started here, after making sure that all models calculate $O_2$ and $H_2O$ photolysis rates accurately.

# 7. Conclusion

In conclusion, we find that the reasons for some of the discrepancies between the WACCM6 model and previous 1-D models of ozone evolution have been resolved, while others have not. The short lifetime of methane at low $pO_2$ ($\leq$ 0.1 PAL) found by C22 [4] is an artefact of WACCM6's neglect of scattering and absorption of solar UV radiation by other gases at wavelengths within the $O_2$

Schumann–Runge bands. This produced tropospheric OH concentrations that were unrealistically high. Thus, the possibility remains that methane could have been an important greenhouse gas during the Proterozoic eon. That said, the Kasting group 1-D model does not handle this problem rigorously, either. Work is underway to correct these deficiencies in both models.

The reasons for the lower ozone column depths calculated by the WACCM6 model compared with those predicted in 1-D are only partly understood. Odd oxygen production, as well as loss processes for $O_3$ like destroying by $NO_x$, $ClO_x$, $HO_x$ in different models should be carefully tested. The use of fixed mixing ratio lower boundary conditions for biogenic trace gases, especially $CH_3Cl$, in WACCM6, as compared with the fixed flux boundary conditions used in the 1-D model, can contribute to some discrepancies on the ozone column depth, but needs more evidence from the other two models to determine whether this is a major factor, or not. But a major part of the discrepancy in ozone column depths could be caused by the different treatments of vertical transport in the two models, along with different methods of parametrizing upper tropospheric $H_2O$ concentrations. If so, the more realistic treatment of convection and transport in the 3-D models should cause those models to be preferred. Future intercomparisons between these and other ozone evolution models are planned to resolve this issue.

**Data accessibility.** All three models are publicly available. The source code for the 1-D photochemical model is available on Github: https://github.com/AoshuangJi/1-D-photochemical-model and has been archived within the Zenodo repository: https://doi.org/10.5281/zenodo.7818127. The specific release for WACCM6 used in this paper is CESM2.1.3, which can be downloaded from the following website: https://escomp.github.io/CESM/versions/cesm2.1/html/downloading_cesm. The ROCKE-3D model is available through: https://simplex.giss.nasa.gov/gcm/ROCKE-3D/. Data are available through the Dryad Dataset: https://doi.org/10.5061/dryad.kh18932b3 [52] and the Zenodo repository: https://doi.org/10.5281/zenodo.7821813 [53].

The data are provided in the electronic supplementary material [54].

**Authors' contributions.** A.J.: conceptualization, formal analysis, investigation, methodology, writing—original draft, writing—review and editing; J.F.K.: conceptualization, formal analysis, funding acquisition, investigation, methodology, project administration, supervision, writing—original draft, writing—review and editing; G.J.C.: formal analysis, investigation, writing—review and editing; D.R.M.: formal analysis, investigation, writing—review and editing; K.T.: investigation, writing—review and editing.

All authors gave final approval for publication and agreed to be held accountable for the work performed therein.

**Conflict of interest declaration.** We declare we have no competing interests.

**Funding.** This work was supported by the Teaching Assistantship from the Department of Geosciences and the Evan Pugh Fund from Penn State. G.J.C. acknowledges the studentship funded by the Science and Technology Facilities Council of the United Kingdom (STFC; grant no. ST/T506230/1). D.R.M. is supported in part by the National Center for Atmospheric Research, which is a major facility sponsored by the National Science Foundation under Cooperative Agreement no. 1852977. K.T. acknowledges support from the Goddard Space Flight Center Sellers Exoplanet Environments Collaboration (SEEC) and ROCKE-3D: The evolution of solar system worlds through time, funded by the NASA Planetary and Earth Science Divisions Internal Scientist Funding Model.

**Acknowledgements.** Thanks to Chester E. Harman for helpful inputs. Also thanks to Rafael Fernández, Gustavo Gerardo Palancar and Orlando Tomazzeli for their help on the line-by-line calculations. The authors want to thank editor Peter Haynes and two anonymous reviewers for their substantial comments on this work. Computer resources for the Kasting group 1-D modelling effort were made available by the College of Earth and Mineral Sciences at Penn State. The WACCM6 simulations were undertaken on ARC4, part of the High Performance Computing facilities at the University of Leeds, UK. Resources supporting this work were also provided by the NASA High-End Computing (HEC) Program through the NASA Center for Climate Simulation (NCCS) at Goddard Space Flight Center.

# References

1. Kasting JF, Donahue TM. 1980 The evolution of atmospheric ozone. *J. Geophys. Res.* **85**, 3255. (doi:10.1029/JC085iC06p03255)
2. Kasting JF, Holland HD, Pinto JP. 1985 Oxidant abundances in rainwater and the evolution of atmospheric oxygen. *J. Geophys. Res. Atmosph.* **90**, 10 497–10 510. (doi:10.1029/JD090iD06p10497)
3. Segura A, Krelove K, Kasting JF, Sommerlatt D, Meadows V, Crisp D, Cohen M, Mlawer E. 2003 Ozone concentrations and ultraviolet fluxes on Earth-Like planets around other stars. *Astrobiology* **3**, 689–708. (doi:10.1089/153110703322736024)
4. Cooke GJ, Marsh DR, Walsh C, Black B, Lamarque J-F. 2022 A revised lower estimate of ozone columns during Earth's oxygenated history. *R. Soc. Open Sci.* **9**, 211165. (doi:10.1098/rsos.211165)
5. Jaziri AY, Charnay B, Selsis F, Leconte J, Lefevre F. 2022 Dynamics of the Great Oxidation Event from a 3D photochemical-climate model. *Clim. Past* **18**, 2421–2447. (doi:10.5194/cp-18-2421-2022)
6. Way MJ *et al.* 2017 Resolving orbital and climate keys of Earth and extraterrestrial environments with dynamics (ROCKE-3D) 1.0: a general circulation model for simulating the climates of rocky planets. *Astrophys. J. Suppl. Ser.* **231**, 12. (doi:10.3847/1538-4365/aa7a06)
7. Liu P, Liu J, Ji A, Reinhard CT, Planavsky NJ, Babikov D, Najjar RG, Kasting JF. 2021 Triple oxygen isotope constraints on atmospheric $O_2$

and biological productivity during the mid-Proterozoic. *Proc. Natl. Acad. Sci. USA* **118**, e2105074118. (doi:10.1073/pnas.2105074118)

8. Toon OB, McKay CP, Ackerman TP, Santhanam K. 1989 Rapid calculation of radiative heating rates and photodissociation rates in inhomogeneous multiple scattering atmospheres. *J. Geophys. Res.* **94**, 16287. (doi:10.1029/JD094iD13p16287)
9. Stanton CL, Reinhard CT, Kasting JF, Ostrom NE, Haslun JA, Lyons TW, Glass JB. 2018 Nitrous oxide from chemodenitrification: a possible missing link in the Proterozoic greenhouse and the evolution of aerobic respiration. *Geobiology* **16**, 597–609. (doi:10.1111/gbi.12311)
10. Ranjan S, Schwieterman EW, Harman C, Fateev A, Sousa-Silva C, Seager S, Hu R. 2020 Photochemistry of anoxic abiotic habitable planet atmospheres: impact of new $H_2O$ cross sections. *Astrophys. J.* **896**, 148. (doi:10.3847/1538-4357/ab9363)
11. Gettelman A *et al.* 2019 The whole atmosphere community climate model version 6 (WACCM6). *J. Geophys. Res. Atmospheres* **124**, 12 380–12 403. (doi:10.1029/2019JD030943)
12. Lin S-J, Rood RB. 1997 An explicit flux-form semi-Lagrangian shallow-water model on the sphere. *Q. J. R. Meteorol. Soc.* **123**, 2477–2498. (doi:10.1002/qj.49712354416)
13. Emmons LK *et al.* 2020 The chemistry mechanism in the community Earth system model version 2 (CESM2). *J. Adv. Model. Earth Syst.* **12**, e2019MS001882. (doi:10.1029/2019MS001882)
14. Emmons LK *et al.* 2010 Description and evaluation of the model for ozone and related chemical tracers, version 4 (MOZART-4). *Geosci. Model Dev.* **3**, 43–67. (doi:10.5194/gmd-3-43-2010)
15. Kinnison DE *et al.* 2007 Sensitivity of chemical tracers to meteorological parameters in the MOZART-3 chemical transport model. *J. Geophys. Res.* **112**, D20302. (doi:10.1029/2006JD007879)
16. Horowitz LW *et al.* 2003 A global simulation of tropospheric ozone and related tracers: description and evaluation of MOZART, version 2. *J. Geophys. Res. Atmospheres* **108**, 4784. (doi:10.1029/2002JD002853)
17. Burkholder JB *et al.* 2015 *Chemical kinetics and photochemical data for use in atmospheric studies: evaluation number 18*. Pasadena CA: Jet Propuls. Lab. Natl. Aeronaut. Space Adm., 1392.
18. Chabrillat S, Kockarts G. 1997 Simple parameterization of the absorption of the solar Lyman-alpha line. *Geophys. Res. Lett.* **24**, 2659–2662. (doi:10.1029/97GL52690)
19. Brasseur GP, Solomon S. 2005 *Aeronomy of the middle atmosphere: chemistry and physics of the stratosphere and mesosphere*. Dordrecht, The Netherlands: Springer.
20. Koppers GAA, Murtagh DP. 1996 Model studies of the influence of $O_2$ photodissociation parameterizations in the Schumann-Runge bands on ozone related photolysis in the upper atmosphere. *Ann. Geophys.* **14**, 68–79. (doi:10.1007/s00585-996-0068-9)
21. Minschwaner K, Siskind DE. 1993 A new calculation of nitric oxide photolysis in the stratosphere, mesosphere, and lower thermosphere. *J. Geophys. Res. Atmosph.* **98**, 20 401–20 412. (doi:10.1029/93JD02007)
22. Allen M, Frederick JE. 1982 Effective photodissociation cross sections for molecular oxygen and nitric oxide in the Schumann-Runge bands. *J. Atmosph. Sci.* **39**, 2066–2075. (doi:10.1175/1520-0469(1982)039<2066:EPCSFM>2.0.CO;2)
23. Eyring V *et al.* 2007 Multimodel projections of stratospheric ozone in the 21st century. *J. Geophys. Res.* **112**, D16303. (doi:10.1029/2006JD008332)
24. Eyring V *et al.* 2010 Sensitivity of 21st century stratospheric ozone to greenhouse gas scenarios. *Geophys. Res. Lett.* **37**, L16807. (doi:10.1029/2010GL044443)
25. Schmidt GA *et al.* 2014 Configuration and assessment of the GISS ModelE2 contributions to the CMIP5 archive. *J. Adv. Model. Earth Syst.* **6**, 141–184. (doi:10.1002/2013MS000265)
26. Edwards JM. 1996 Efficient calculation of infrared fluxes and cooling rates using the two-stream equations. *J. Atmosph. Sci.* **53**, 1921–1932. (doi:10.1175/1520-0469(1996)053<1921:ECOIFA>2.0.CO;2)
27. Edwards JM, Slingo A. 1996 Studies with a flexible new radiation code. I: choosing a configuration for a large-scale model. *Q. J. R. Meteorol. Soc.* **122**, 689–719. (doi:10.1002/qj.49712253107)
28. Houweling S, Dentener F, Lelieveld J. 1998 The impact of nonmethane hydrocarbon compounds on tropospheric photochemistry. *J. Geophys. Res. Atmosph.* **103**, 10 673–10 696. (doi:10.1029/97JD03582)
29. Shindell DT, Grenfell JL, Rind D, Grewe V, Price C. 2001 Chemistry-climate interactions in the Goddard Institute for Space Studies general circulation model: 1. Tropospheric chemistry model description and evaluation. *J. Geophys. Res. Atmosph.* **106**, 8047–8075. (doi:10.1029/2000JD900704)
30. Shindell DT, Faluvegi G, Bell N. 2003 Preindustrial-to-present-day radiative forcing by tropospheric ozone from improved simulations with the GISS chemistry-climate GCM. *Atmosph. Chem. Phys.* **3**, 1675–1702. (doi:10.5194/acp-3-1675-2003)
31. Shindell DT, Faluvegi G, Unger N, Aguilar E, Schmidt GA, Koch DM, Bauer SE, Miller RL. 2006 Simulations of preindustrial, present-day, and 2100 conditions in the NASA GISS composition and climate model G-PUCCINI. *Atmosph. Chem. Phys.* **6**, 4427–4459. (doi:10.5194/acp-6-4427-2006)
32. Hunten DM. 1975 Estimates of stratospheric pollution by an analytic model. *Proc. Natl Acad. Sci. USA* **72**, 4711–4715. (doi:10.1073/pnas.72.12.4711)
33. Massie ST, Hunten DM. 1981 Stratospheric eddy diffusion coefficients from tracer data. *J. Geophys. Res.* **86**, 9859. (doi:10.1029/JC086iC10p09859)
34. National Research Council. 1976 *Halocarbons: effects on stratospheric ozone*. Washington, DC: National Academies Press.
35. Braesicke P, Neu JL, Fioletov VE, Godin-Beekmann S, Hubert D, Petropavlovskikh I, Shiotani M, Sinnhuber B-M. 2019 Update on global ozone: past, present, and future. In *Scientific assessment of ozone depletion: 2018, global ozone research and monitoring project—report no. 58* (eds W Steinbrecht, M Weber), chapter 3, p. 74. World Meteorological Organization.
36. McClatchey R, Fenn R, Volz F, Garing J. 1971 Optical properties of the atmosphere (revised). *Environ. Res. Pap.* **411**, 100. (doi:10.1029/95JB03048)
37. Cronin TW. 2014 On the choice of average solar zenith angle. *J. Atmosph. Sci.* **71**, 2994–3003. (doi:10.1175/JAS-D-13-0392.1)
38. Manabe S, Wetherald RT. 1967 Thermal equilibrium of the atmosphere with a given distribution of relative humidity. *J. Atmosph. Sci.* **24**, 241–259. (doi:10.1175/1520-0469(1967)024<0241:TEOTAW>2.0.CO;2)
39. Ratner MI, Walker JCG. 1972 Atmospheric ozone and the history of life. *J. Atmosph. Sci.* **29**, 803–808. (doi:10.1175/1520-0469(1972)029<0803:AOATHO>2.0.CO;2)
40. Fernández RP, Palancar GG, Madronich S, Toselli BM. 2007 Photolysis rate coefficients in the upper atmosphere: effect of line by line calculations of the $O_2$ absorption cross section in the Schumann–Runge bands. *J. Quant. Spectrosc. Radiat. Transf.* **104**, 1–11. (doi:10.1016/j.jqsrt.2006.08.005)
41. Marsh DR, Garcia RR, Kinnison DE, Boville BA, Sassi F, Solomon SC, Matthes K. 2007 Modeling the whole atmosphere response to solar cycle changes in radiative and geomagnetic forcing. *J. Geophys. Res. Atmosph.* **112**, D23306. (doi:10.1029/2006JD008306)
42. Spivakovsky CM *et al.* 2000 Three-dimensional climatological distribution of tropospheric OH: update and evaluation. *J. Geophys. Res. Atmosph.* **105**, 8931–8980. (doi:10.1029/1999JD901006)
43. Kirschke S *et al.* 2013 Three decades of global methane sources and sinks. *Nat. Geosci.* **6**, 813–823. (doi:10.1038/ngeo1955)
44. Graham RJ, Shaw TA, Abbot DS. 2019 The snowball stratosphere. *J. Geophys. Res. Atmosph.* **124**, 11 819–11 836. (doi:10.1029/2019JD031361)
45. Deitrick R, Goldblatt C. 2022 Effects of ozone levels on climate through Earth history. *EGUsphere* 1–27 [Preprint]. (doi:10.5194/egusphere-2022-1158)
46. Fang T-M, Wofsy SC, Dalgarno A. 1974 Opacity distribution functions and absorption in Schumann-Runge bands of molecular oxygen. *Planet. Space Sci.* **22**, 413–425. (doi:10.1016/0032-0633(74)90074-9)
47. Minschwaner K, Salawitch RJ, McElroy MB. 1993 Absorption of solar radiation by $O_2$: implications for $O_3$ and lifetimes of $N_2O$, $CFCl_3$, and $CF_2Cl_2$. *J. Geophys. Res. Atmosph.* **98**, 10 543–10 561. (doi:10.1029/93JD00223)
48. Neu JL, Prather MJ, Penner JE. 2007 Global atmospheric chemistry: Integrating over fractional cloud cover. *J. Geophys. Res.* **112**, D11306. (doi:10.1029/2006JD008007)
49. Mlawer EJ, Taubman SJ, Brown PD, Iacono MJ, Clough SA. 1997 Radiative transfer for inhomogeneous atmospheres: RRTM, a validated correlated-k model for the longwave. *J. Geophys. Res. Atmosph.* **102**, 16 663–16 682. (doi:10.1029/97JD00237)

50. Kato S, Ackerman TP, Mather JH, Clothiaux EE. 1999 The k-distribution method and correlated-k approximation for a shortwave radiative transfer model. *J. Quant. Spectrosc. Radiat. Transf.* **62**, 109–121. (doi:10.1016/S0022-4073(98)00075-2)
51. Harman CE, Felton R, Hu R, Domagal-Goldman SD, Segura A, Tian F, Kasting JF. 2018 Abiotic $O_2$ levels on planets around F, G, K, and M Stars: effects of lightning-produced catalysts in eliminating oxygen false positives. *Astrophys. J.* **866**, 56. (doi:10.3847/1538-4357/aadd9b)
52. Ji A, Kasting JF, Cooke GJ, Marsh DR, Tsigaridis K. 2023 Data from: Comparison between ozone column depths and methane lifetimes computed by one-dimensional and three-dimensional models at different atmospheric $O_2$ levels. Dryad Digital Repository. (doi:10.5061/dryad.kh18932b3)
53. Ji A, Kasting JF, Cooke GJ, Marsh DR, Tsigaridis K. 2023 Code for: Comparison between ozone column depths and methane lifetimes computed by one-dimensional and three-dimensional models at different atmospheric $O_2$ levels. *Zenodo*. (doi:10.5281/zenodo.7821813)
54. Ji A, Kasting JF, Cooke GJ, Marsh DR, Tsigaridis K. 2023 Comparison between ozone column depths and methane lifetimes computed by one-dimensional and three-dimensional models at different atmospheric $O_2$ levels. Figshare. (doi:10.6084/m9.figshare.c.6617700)